***Journal of Cancer Therapy*, 2009, 1, 1-8**

Tissue Sensing Adaptive Radar for Breast Cancer Detection—Experimental Investigation of Simple Tumor Models

ABSTRACT

Microwave breast cancer detection is based on differences in electrical properties between healthy and malignant tissues. Tissue sensing adaptive radar (TSAR) has been proposed as a method of microwave breast imaging for early tumor detection.TSARsenses all tissues in the volume of interest and adapts accordingly. Simulation results have shown the feasibility of this system for detecting tumors of 4mmin diameter. In this paper, the second generation experimental system for TSAR is presented. Materials with electrical properties similar to those in the breast are used for the breast model. A resistively loaded Wu–King monopole antenna is fabricated, and reflections from the breast model over the frequency range of 1–10 GHz are recorded. The reflected signals are processed with the TSAR algorithm, which includes improved skin subtraction and TSAR focusing algorithms. Various tumormodels are examined; specifically, a 1-cm tumor is detected with a signal-to-clutter ratio of 10.41 dB. Tumor detection with the experimental systemis evaluated and compared to simulation results.

Keywords: *breast cancer detection, experimental verification, microwave imaging, tissue sensing adaptiveradar.*

1. Introduction

BREAST cancer is a significant health issue for women and affects one in every seven women [1]. The current method of detection is mammography, which involves X-ray imaging of a compressed breast. X-raymammography creates images of the density of breast tissues and the images are used to locate suspicious areas. Although mammography is the gold standard, concerns related to the false-positive and false-negative rates exist [2]. There is need for a complementary, safe, and reasonably priced method [3]. Microwave breast cancer detection has been introduced as a complementary method for breast cancer detection.

Microwave breast cancer detection relies on differences in electrical properties between malignant and fatty tissues as summarized in [4]. Microwave breast imaging methods include hybrid, passive, and active approaches. Hybrid methods include thermoacoustic tomography, which uses microwaves to selectively heat tumors and ultrasound approaches to create images [5–7]. One passive approach, microwave radiometry, measures the increased temperature of the tumor compared to the normal tissue [7–9]. Active microwave approaches include tomography and radar-based imaging. Microwave tomography records the transmission of waves through the breast and creates an electrical property map of the region of interest [7]. Radar-based approaches, first presented by Hagness et al. [10], involve focusing reflections from the breast in order to determine the location of significant scatterers (i.e., tumors). Radar-based imaging systems include microwave imaging viaspace time (MIST) beamforming [11,12] and tissue sensing adaptive radar (TSAR) [13,14]. The MIST system features a woman lying supine with the antennas scanned over the naturally flattened breast. In the TSAR system, the woman lies prone, the breast falls through a hole in the examination table, and antennas are scanned around the breast. The MIST system uses advanced clutter reduction algorithms to create an image. Simulations have shown that the MIST system can detect a 2-mm tumor in a two-dimensional (2-D) breast model derived from magnetic resonance imaging [11]. The TSAR algorithm uses simple clutter reduction methods; however, tumors of 4 mm have been detected in a three-dimensional (3-D) cylindrical breast model [15].

The experimental verification of each imaging system is the next step before their clinical application. In a realistic system, practical issues such as antenna fabrication, the electrical properties of breast tissues, and breast shape must be considered. The first experimental system for testing radar-based breast cancer detection was presented in [16]. This system was designed for preliminary method verification and included a polyvinyl chloride (PVC) pipe, wood, and air to represent the breast, tumor, and fatty tissues, respectively. The materials used had similar contrasts in electrical properties to those expected in the breast. Detection of a 3-mm-diameter wooden dowel was possible in a 2-D experiment. A quasi-3-D system was presented in [17] and showed detection of a 3-D tumor in a 2-D model. Experimental verification was presented in [12] for the MIST system. The breast model consisted of a printed circuit board (skin), diacetin-water solution (tumor), and soybean oil (fatty tissue). The materials were chosen based on availability, cost, toxicity, and stability. Because the soybean oil has lower dielectric properties than the actual fatty tissue, the materials selected for the skin and tumor were correspondingly lower in properties. Tumors of 4-mm diameter were detected in a 6 cm 6 cm breast model scanned at 49 antenna locations. While this system is more complex than the first-generation experimental TSAR system, the electrical properties are again based on the property contrasts. Therefore, the goal of the second-generation experimental TSAR system is to use materials with electrical properties similar to realistic breast tissues.

This paper reports the experiments and results with the second-generation TSAR prototype. Specifically, it expands on the preliminary results presented in [18], where a 1-cm tumor immersed in canola oil was detected. The aims of this paper are to test and characterize an antenna, implement an improved TSAR algorithm, and detect tumors in a realistic breast model. Section II discusses the experimental system, including the materials used for the breast model and antenna fabrication. The improved signal processing for the skin subtraction algorithm and the TSAR focusing algorithm is presented in Section III. In Section IV, the tumor detection results are presented for various breast models. Section V draws conclusions based on the results and outlines future work with the experimental TSAR system.

2. Experimental System

This section describes the TSAR experimental system. The experimental setup, equipment used, and data acquisition techniques are outlined. As well, the electrical properties of each material in the breast model are discussed. Finally, a description of the antenna fabrication is presented.

2.1 Experimental Setup

The experimental system is shown in Figure 1. The system is composed of a Plexiglas tank, immersion liquid, ground plane, antenna, and breast phantom. The top of the tank is a ground plane, which is implemented to simplify the antenna design. This places limitations on the imaging capabilities of the system; however, this setup is similar to preliminary simulations in [19]. Therefore, it is acceptable for preliminary experimental tests. Holes are placed in the ground plane for placement of the antenna, breast model, and tumors. The entire tank, with the exception of the ground plane, is fabricated without metal, thus reducing reflections from the tank. The dimensions are shown in Figure 2.

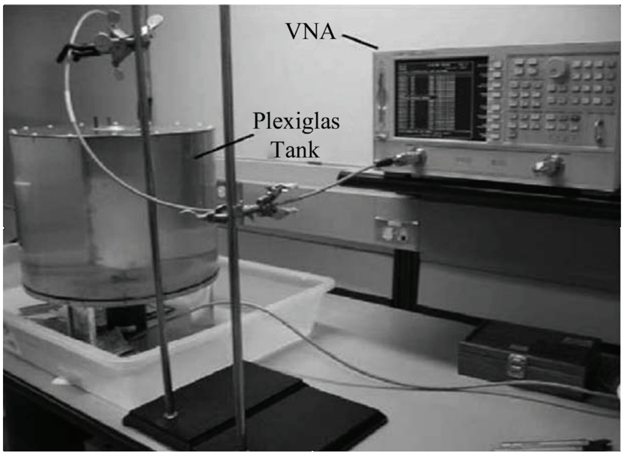

Figure 1. TSAR experimental system. The tank is shown on the left and theVNA is on the right. The coaxial cable is held ith stands to reduce flex and movement

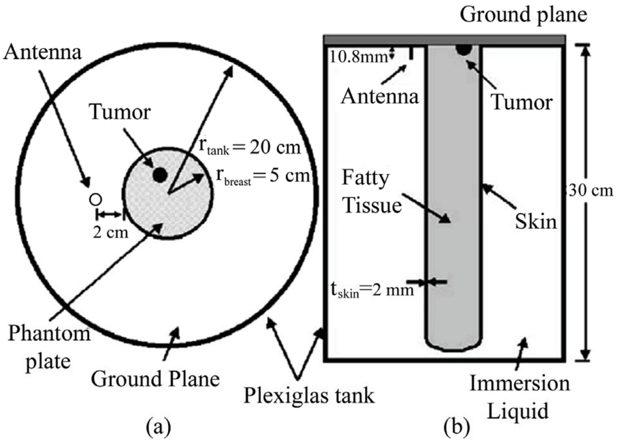

Figure 2. Test setup with a monopole antenna, immersion liquid, and breast phantom. (a) Top-down view. (b) Side view

In all experiments, reflections from the antenna （S_{11}） are recorded with an 8719ES vector network analyzer (VNA) (Agilent Technologies, Palo Alto, CA) connected to a 50-Ω coaxial cable. Data are recorded at 1601 frequency points and 16 samples are averaged at each frequency. The frequency range over which data are acquired is from 1 to 10 GHz. In the experiments, the phantom plate (Figure 2) is rotated in increments of 22.5° or 45°. These rotations are performed to simulate scanning the antenna around the tumor or breast model. Reflections are recorded after each rotation.

2.2. Phantom Materials

The breast model is represented by a cylinder with a diameter of 10 cm and a height of 30 cm. A hemispherical tumor is attached to the ground plane and placed in the breast model, as shown in Figure 2. Here, the length of the breast model is selected such that the antenna does not detect the end of the model (i.e., via method of images, this represents a 2-D model). However, the tumor is 3-D in order to provide a more challenging detection task, as the imaging task involves detecting the 3-D tumor in a plane perpendicular to the cylinder axis and containing the tumor. The breast model is composed of materials with similar electrical properties to skin, fatty tissue, and tumors. The properties of each material are measured using an open-ended borosilicate dielectric probe [20]. The results are summarized in Figure. 3 and Table I.

The skin is composed of a flexible silicone sheet loaded with dielectric fillers named LDF-32 (Eccosorb) (Emerson and CummingMicrowave Products, Randolph, MA). The electrical properties of the skin are shown in Figure. 3. The sheet of material is formed into a cylinder by joining the sheet with TP-50 epoxy (Eccobond TP-50) (Emerson and Cumming Microwave Products). This epoxy has electrical properties of $\varepsilon_r = 4$ and $\sigma = 0.04$ S/m at 4 GHz; however, this value may vary as air microbubbles are dispersed throughout the material. The fatty tissue is created from flour, canola oil, and 0.9% saline [21] in a ratio by weight of 500 : 225 : 25. The fatty tissue mixture is a dough that is packed in the interior of the skin cylinder. The electrical properties of the fat dough (Figure 3) were monitored for a three-week period. The electrical properties decreased by 10% as the water evaporated. As a first approximation, the electrical properties are selected to represent mainly the fatty tissue inside the breast and hence have lower permittivity than the average properties used in [10].

Tumors are fabricated using Alginate powder (Alginmax) (Major Proditti Dentari S.P.A., Moncalieri, Italy), water, and salt in a ratio by weight of 115:250:14 [22]. The tumors are covered with a thin layer of epoxy (Eccostock HiK cement) (Emerson and Cumming Microwave Products). The epoxy (and S/m) creates a layer between the oil and the tumor to prevent diffusion of the tumor in the oil. Furthermore, this conserves the electrical properties (Figure 3) of the tumor. Over a three-week period, measurements demonstrated minimal change in properties. The thickness of the epoxy layer is difficult to control; however, the size of the tumor is measured based on the tumor and epoxy size combined. Therefore, as investigated in [18], the epoxy layer reduces reflections from the tumor, which creates a more difficult tumor detection scenario. As described in [18], the tumors are attached to metal plugs and inserted into the ground plane of the tank.

An immersion liquid is needed to improve the match between interior and exterior of the breast. Therefore, the tank is filled with an immersion liquid of canola oil ($\varepsilon_r = 2.5$, $\sigma = 0.04$ S/m). Canola oil is similar to the liquid investigated in [14], which provides excellent tumor detection and localization. Additionally, fewer antennas are required to scan a given volume than with a higher permittivity liquid [14]. Furthermore, canola oil is minimally dispersive over the frequency range of interest and has low loss.

The electrical properties of the breast model at 4 GHz are listed in Table I. The materials have a relatively small change in permittivity over the frequency range (Figure 3) and the changes correspond to those observed in real tissues (e.g., [23]). Furthermore, the materials used to represent the breast have similar electrical properties to those of real tissues [7].

2.3. Antenna Fabrication

The antenna used to illuminate the breast model is a resistively loaded Wu–King monopole [24, 25]. The resistively loaded monopole is selected as it provides acceptable performance over the ultrawideband frequency range of interest. The monopole has length of 10.8 mm and is designed in a lossless liquid similar to oil with $\varepsilon_r = 3.0$. The design and characterization of the antenna are out-

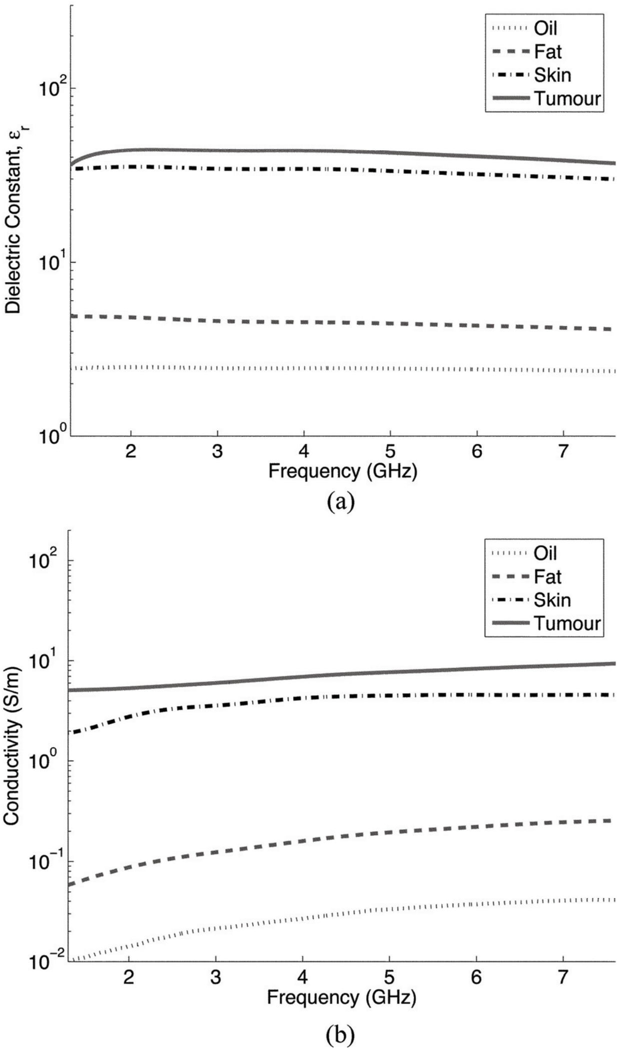

(a)

(b)

Figure 3. Electrical properties of materials in the breast model. All properties are measured with an open-ended borosilicate dielectric probe [20]. (a) Relative permittivity and (b) conductivity as a function of frequency

Table 1. Electrical properties used in the experimental system. All materials are measured with an open-ended borosilicate dielectric probe [20] at 4 ghz

Object	Permittivity, ϵ_r	Conductivity, σ(s/m)
Canola Oil	2.5	0.04
Fatty Tissue	4.2	0.16
Skin	34.3	4.25
Tumor	43.7	6.94

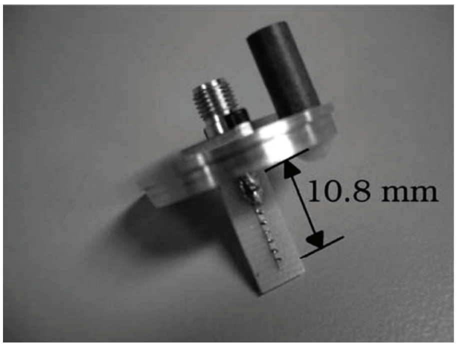

Figure 4. Fabricated Wu–King monopole antenna soldered to an SMA connector and attached to a metal plug

lined in [14] and [18]. The antenna is fabricated using high-frequency chip resistors (Vishay 0603HF) (Rogers RO3203 series) (Rogers Corporation, Chandler, AZ). The substrate ($\mathcal{E}_r = 3.02$ and $\sigma = 0.001$ S/m) has electrical properties similar to those of the canola oil.

The antenna is soldered to a subminiature A (SMA) connector and attached to a metal plug. The fabricated antenna (Figure 4) is inserted into the ground plane of the tank.

3. Signal Processing

The signal processing includes converting signals from frequency to time, and the TSAR image formation algorithm. Theinitial signal processing step is converting the frequency-domain data to the time domain for use in the image formation algorithms. As in [16], the measured data are weighted with a differentiated Gaussian signal with center frequency of 4 GHz and full-width half maximum extent from 1.3 to 7.6 GHz. The data are transformed with an inverse chirp *z* transform to produce thetime-domain signal.

The TSAR image formation algorithm is similar to that of [16]; however, improvements to the skin subtraction and focusing step are implemented. The first step is calibration, which involves subtracting the reflections recorded without an object present. This removes clutter in the signals, such as reflections from the Plexiglas tank. The remaining signal contains antenna mismatch, skin reflection, and tumor reflection. The next steps in the TSAR algorithm are skin subtraction and focusing, discussed in this section.

3.1. Skin Subtraction

The skin subtraction algorithm previously implemented was an adaptive correlation method named Woody averaging [13,26]. This method provided effective skin subtraction; however, a residual skin response remained. Therefore, an improved skin subtraction algorithm is desired.

The proposed skin subtraction algorithm is based on the recursive least squares (RLS) algorithm, which is an adaptive filtering method. The method is adapted from a beamformer approach in [27]. A single signal is selected as the target signal and the remaining signals are weighted and summed to approximate the target signal. The desired signal is defined as u_r or d, a $1 \times N$ vector where $d(i)$ is the sample at time i. The input signal or remaining ignals can be defined as $u = [u_r + 1, u_r + 2, \cdots u_r + Q]^T$ and is a $Q \times N$ matrix where Q is the number of input signals. The weight vector at time n is defined as $w(n) = \left[w_r + 1(n), w_r + 2(n), \cdots w_r + Q(n)\right]^T$ and is a $Q \times 1$ vector. The approximation to the desired signal at time i is defined as

$$\widehat{d}(i) = y(i) = w^T(n)u(i) \tag{1}$$

and the error in the approximation is calculated as

$$e(i) = d(i) - \widehat{d}(i) \tag{2}$$

At time , the sum of the squared error is defined as

$$J(n) = \sum_{i=1}^{n} \lambda^{n-1} \left|e(i)\right|^2 \tag{3}$$

where is the forgetting factor and is the current sample number. Expanding to include the definition of results in

$$\begin{aligned} J(n) = {} & \sum_{i=1}^{n} \lambda^{n-1} d^2(i) - 2w^T(n) \sum_{i-1}^{n} \lambda^{n-1} u(i) d^T(i) \\ & + w^T(n) \left[\sum_{i=1}^{n} \lambda^{n-1} u(i) u^T(i) \right] w(n) \end{aligned} \tag{4}$$

Defining

$$D(n) = \sum_{i=1}^{n} \lambda^{n-1} d^2(i) \tag{5}$$

$$F(n) = \sum_{i=1}^{n} \lambda^{n-1} u(i) u^T(i) \tag{6}$$

$$z(n) = \sum_{i=1}^{n} \lambda^{n-1} u(i) d^T(i) \tag{7}$$

permits us to write $J(n)$ as

$$J(n) = D(n) - 2w^T(n)z(n) + w^T(n)F(n)w(n) \tag{8}$$

Minimization of the mean squared error with respect to results in the basic Wiener–Holf equation

$$F(n)w(n) = z(n) \tag{9}$$

Solving for $w(n)$ recursively using the standard brute force approach equates

$$F(n) = \lambda F(n-1) + w(n)u^T(n) \tag{10}$$

and

$$z(n) = \lambda z(n-1) + w(n)d^T(n) \tag{11}$$

However, to solve (9) requires a matrix inversion.

Therefore, the matrix inversion lemma is used to solve for $F^{-1}(n)$ as in[27].

This method differs from the MIST skin subtraction approach presented in [11], as the weight vectors are updated recursively after each time step. In contrast, the method proposed in [11] has a constant weight vector, which is shifted through the selected window.

When applied to TSAR signals, the RLS algorithm and Woody averaging methods are combined. The RLS algorithm estimates the skin response and is therefore applied from the start of the signal to a point corresponding to the interior of the breast. This is obtained from the skin location and thickness estimates [28]. The Woody averaging algorithm is applied from the interior of the breast to the remaining portion of the signal. Therefore, signals estimated with the RLS algorithm and Woody averaging are combined, creating a total estimated signal. The total estimated signal is subtracted from the target signal. This process is repeated with the signal received at each antenna as the target signal.

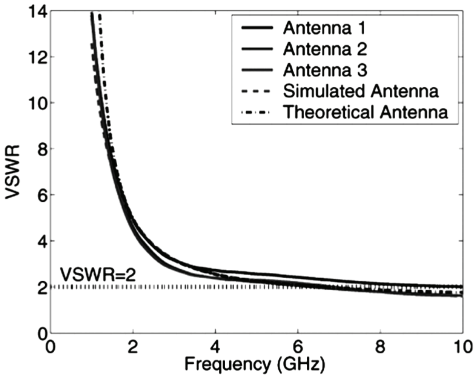

Figure 5. Experimental, simulated, and theoretical VSWR calculated from the reflection coefficient [18]

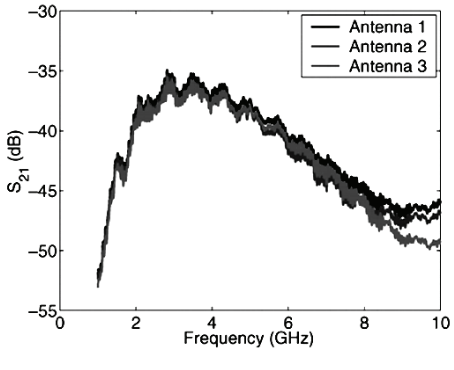

Figure 6. Transmission between two antennas (S_{21})

3.2. Focusing

The skin-subtracted signals are integrated and focused similar to [28]. The focusing is performed by identifying a focal point inside the region bounded by the synthetic antenna array and calculating the travel time from each antenna to the focal point. The selected contribution from each signal is summed and the process is repeated as the focal point is scanned through the focusing region. The resulting image indicates the location of significantly scattering objects as reflections from these objectsadd coherently [16]. To improve selectivity of focus, several additions are made to the algorithm [29]. Mathematically, pixel intensity at location can be described by

$$p(i,j,k) = \left(\sum_{n} s(i,j,k,n) w(i,j,k,n) Q(i,j,k,n) \right)^2 \tag{12}$$

The contribution from antenna n, $s(i,j,k,n)$, is identified using the travel time between the antenna and the pixel location. Weighting $w(i,j,k,n)$ gives more weight to the antennas closest to the current focal point. Signal compensation $Q(i,j,k,n)$ includes variable compensation $(v(i,j,k,n))$ and in-breast compensation $(d_{tissue}(i,j,k,n))$

$$Q(i,j,k,n) = v(i,j,k,n) d_{tissue}(i,j,k,n) \tag{13}$$

In-breast compensation $d_{tissue}(i,j,k,n)$ is the distance traveled in breast tissue and is determined using the estimated skin location. Variable compensation $v(i,j,k,n)$ has a value of zero if the pixel location is outside of the skin, one if the location is between the skin and the array center, and decreases as $1/\gamma$ if the location is beyond the array center, where γ is the distance from the antenna. The skin location is calculated as in [28]. The images are evaluated using the signal-to-clutter ratio. The signal-to-clutter ratio is calculated as the maximum tumor response compared to the maximum response in the same image with the tumor response removed [28].

4. Results and Discussion

4.1. Antenna

Three antennas are fabricated with the same profile and compared to simulations to confirm correct operation.

The impedance of the simulated antenna in [14] is converted to represent a monopole. The theoretical impedance is calculated from [30]. The voltage standing wave ratios (VSWRs) for the fabricated, simulated, and theoretcal antennas are shown in Figure 5. The results demonstrate a good match between all fabricated antennas and the simulated antenna. The VSWR is below 2 between 7–10 GHz. The poor VSWRs at lower frequencies are expected as matching to 50 Ω was not a design goal. However, the input impedance of the antenna is relatively constant over the frequency range of interest and the design of an impedance transformer is feasible.

Transmission between two antennas is measured by connecting an antenna to each port of the VNA and measuring S_{21}. The antennas are placed in the immersion liquid and separated by 7 cm as this is sufficiently in the far field of the antennas. Transmission S_{21} is measured using the same reference antenna, which is similar to the antennas in Figure 5. The results demonstrate a transmission of approximately 38 dB at 4 GHz as shown in Figure 6. This low transmission can be attributed to the poor VSWR and the resistive profile of the antenna. The decrease in transmission at higher frequencies may be in part due to the variation in resistors at higher frequencies.

The efficiency of the antenna is calculated using definitions in [31] and finite-difference time-domain (FDTD) simulations. Specifically, we compute the power radiated through a closed surface surrounding the antenna and divide this by the input power. The efficiency ranges from 1.9% to 15.8% over the frequency range from 2 to 8 GHz. At maximum power of 5 dBm from the VNA, the total power radiated at 4 GHz is -6.2 dBm. Although this antenna has poor performance, it is still implemented for tumor detection due to simplicity. Furthermore, if tumor detection is possible with an inefficient antenna, improved detection capabilities are expected with an improved antenna.

4.2. Tumor Detection and Skin Subtraction

In a preliminary experiment, a tumor was placed in the immersion liquid and rotated around the center of the tank. Reflections were recorded at eight antenna positions and imaged with the focusing algorithm [18]. The tumor was clearly detected with maximum response located at $x = 7.4$ cm and $y = 6.9$ cm while the actual physical location was $x = 7.5$ cm and $y = 7.0$ cm. The signal-to-clutter ratios were 8.21 and 7.19 dB for the 2- and 1-cm tumors, respectively. The signal-to-clutter ratio decreased with tumor size, as expected. The results were promising as tumor detectionwas possible with very little clutter [18].

The next experiment includes the skin and the interior of the skin filled with canola oil. The two skin subtraction algorithms, Woody averaging and the RLS–Woody combination, are applied to the data and the skin response is compared before and after skin subtraction. Figure 7 demonstrates the effectiveness of the RLS algorithm compared to the Woody averaging results. The peak-to-peak of the skin response is calculated prior to and after skin subtraction, and the ratio of these quantities is calculated.

Here, the peak-to-peak results are -26.33 and -107.87 dB for Woody averaging and the RLS algorithm, respectively. The skin-subtracted data recorded at 15 antenna positions are focused using the TSAR focusing algorithm.

The signal-to-clutter ratios for a 1-cm tumor are calculated to be 6.63 dB forWoody averaging and 14.37 dB for the RLS–Woody combination. These results further demonstrate the effectiveness of the RLS–Woody combination, which is selected as the skin subtraction method for the remainder of this paper.

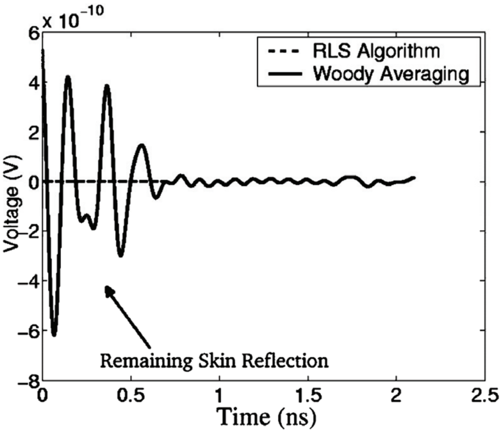

Figure 7. Plot of a single skin-subtracted response using the Woody averaging method and the RLS algorithm. This shows the effectiveness of the RLS skin subtraction method

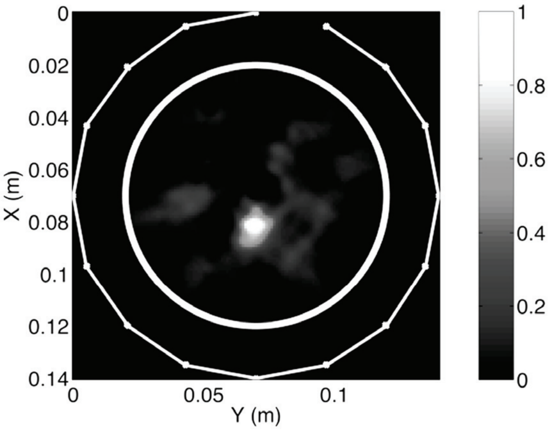

Figure 8. Image of 1-cm tumor in the complete breast model. The white circle is a postprocessing step to illustrate the actual location of the skin cylinder. The exterior line represents the antenna locations. Strongly scattering objects are indicated with lighter intensities while darker pixels indicate areas of weak scattering

4.3. TSAR Images

The final experiment is the most complex and includes the skin, tumor, and fatty tissue. Reflections are recorded and the TSAR algorithm is applied to the data. The resul-ts are plotted in Fig. 8 for a 1-cm tumor. The tumor is detected with maximum response located at $x = 8.1$ cm and $y = 6.9$ cm, while the physical location is $x = 8.0$ cm and $y = 7.0$ cm. The signal-toclutter ratios are 13.74 and 10.41 dB for the 2- and 1-cm tumors, respectively. To confirm and compare the results, simulations are performed with the FDTD method [32]. The simulation setup is as in [14]; however, the breast interior is homogeneous, and material properties are the same as discussed in Section 2. The recorded reflections from the simulations are focused, and the signal-to-clutter ratio for the 1-cm tumor is 23.38 dB. As expected, the signal-to-clutter ratio is higher for simulations than experi-

Table 2. Signal-to-clutter ratios for each breast model

Tumor Size (cm)	Tumor Only (dB)	Skin-Tumor (dB)	Skin-Fat-Tumor (dB)
2	8.21	14.51	13.74
1	7.19	14.37	10.41CCCC

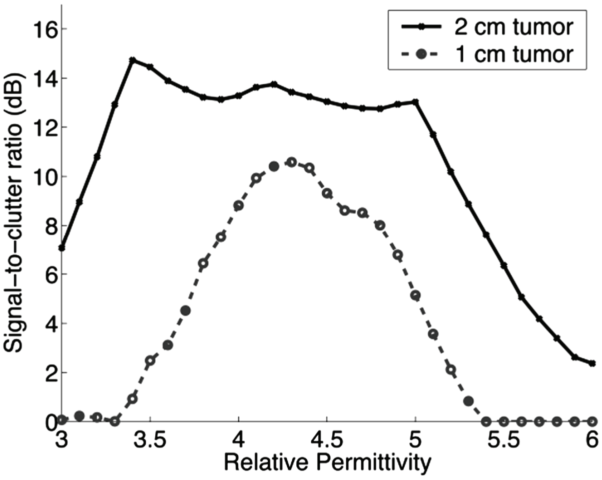

Figure 9. Signal-to-clutter ratio received when changing the permittivity in the TSAR focusing algorithm. The highest signal-to-clutter ratios occur when the permittivity value used for calculation is the same as the measured value

ments. Simulations provide a relatively noise-free environment and a homogeneous breast interior. In addition, oscillations are introduced in the measured signal when converting from the frequency to the time domain, as the weighting function is band limited.

The signal-to-clutter ratios for each of the three experiments are shown in Table II. As expected, the signal-to-clutter ratio decreases as the tumor size decreases. The tumor-only simulations have low signal-to-clutter ratios compared to the skin tumor case as only eight antenna positions are used to create an image. Finally, as the complexity of the system increases, the signal-to-clutter ratios decrease.

These results are promising, as tumor detection is possible using an inefficient antenna to record the reflections. Therefore, with an improved antenna, improved tumor detection capability is anticipated.

Finally, the robustness of the algorithm to changes in breast permittivity is tested. The permittivity of the fatty tissue in the interior of the breast is varied from 3 to 6 in the postprocessing algorithm. This variation changes the travel time from the antenna to focal point. The signal-to-clutter ratios are calculated as the permittivity values are changed in 0.1 increments and shown in Figure 9. The results indicate that, for small tumors, the largest signal-to-clutter ratio is obtained when the electrical properties are similar to the measured value of the fatty tissue. This demonstrates the necessity of prior information on the electrical properties inside the breast to achieve the highest signal-to-clutter ratio. In the case of inhomogeneous breast tissue, an average permittivity value is necessary to compute the travel time through the breast tissue. Algorithms for estimating the average permittivity in the breast have been introduced in [33]. With an estimate of the average properties, the focusing algorithms described here have detected tumors in simple breast models containing variations in properties of 10% [14].

5. Conclusions

This paper presents the second-generation TSAR experimental system. The materials used to represent the breast and the corresponding electrical properties were presented. The RLS algorithm was introduced as an improved skin subtraction algorithm compared to the previous method of Woody averaging. Tumor detection and localization were possible in three breast phantoms of increasing complexity. These results are promising as the materials used to represent the breast have similar electrical properties to those in a realistic breast. Furthermore, this is the most complex breast model currently under investigation for radar-based tumor detection. The tumors examined here are larger in diameter than the 4-mm tumors detected with a 3-D model reported in [14]. Testing detection of smaller tumors is planned with a 3-D system.

Although promising results are obtained with this simpl system, experiments in 3-D are not performed. Currently,the antenna is the limiting factor for 3-D experiments. An improved antenna is under development, and improved performance and directivity are expected. This should increase the tumor detection capabilities of the TSAR system. Another challenge is the development of a 3-D breast model, including more realistic shape and inhomogeneities. The materials and methods reported here may be used to develop this realistic model. Finally, a scanning system must be developed to scan the improved antenna around the new model. This may involve a vertical scan in addition to the rotation of the model reported here. Therefore, this paper with a simple model provides a foundation for expansion to a 3-D system.

6. Acknowledgments

The authors would like to acknowledge the technical support of S. Foster, I. Choi, F. Hickli, and J. Shelley, all of the University of Calgary, Calgary, AB, Canada.

REFERENCES

[1] American Cancer Society, “Cancer facts and figures 2005,” Amer. Cancer Soc,, Atlanta, GA, 2005.

[2] Mammography and Beyond: Developing Technologies for the Early Detection of Breast Cancer. Washington, DC: Inst. Med., Nat. Academy Press, 2001.

[3] Saving Women’s Lives: Strategies for Improving Breast Cancer Detection and Diagnosis. Washington, DC: Inst. Med., Nat. Academy Press,2004.

[4] E. C. Fear, “Microwave imaging of the breast,” Technol. Cancer Res. Treat., vol. 4, no. 1, pp. 69–82, Feb. 2005.

[5] R. A. Kruger, K. K. Kpoecky, A. M. Aisen, D. R. Reinecke, G. A. Kruger, and W. L. Kiser Jr., "Thermoacoustic CT with radio waves: A medical imaging paradigm," Radiology, vol. 211, no. 1, pp. 275–278, 1999.

[6] L. V. Wang, X. Zhao, H. Sun, and G. Ku, "Microwave-induced acoustic imaging of biological tissues," Rev. Sci. Instrum., vol. 70, no. 9, pp. 3744–3748, 1999.

[7] E. C. Fear, S. C. Hagness, P. M. Meaney, M. Okoniewski, and M. A. Stuchly, "Enhancing breast tumor detection with near-field imaging," IEEE Micro, vol. 3, no. 1, pp. 48–56, Mar. 2002.

[8] S. Mouty, B. Bocquet, R. Ringot, N. Rocourt, and P. Devos, "Microwave radiometric imaging for the characterization of breast tumors," Eur. Phys. J.: Appl. Phys., vol. 38, pp. 73–78, 2000.

[9] K. L. Carr, P. Cevasco, P. Dunlea, and J. Shaeffer, "Radiometric sensing: An adjuvant to mammography to determine breast biopsy," in IEEE MTT-S Int. Microwave Symp. Dig., Boston, MA, Jun. 2000, pp. 929–932.

[10] S. C. Hagness, A. Taflove, and J. E. Bridges, "Two-dimensional FDTD analysis of a pulsed microwave confocal system for breast cancer detection: Fixed-focus and antenna-array sensors," IEEE Trans. Biomed. Eng., vol. 45, no. 12, pp. 1470–1479, Dec. 1998.

[11] E. J. Bond, X. Li, S. C. Hagness, and B. D. Van Veen, "Microwave imaging via space time beamforming for early detection of breast cancer," IEEE Trans. Antennas Propag., vol. 51, no. 8, pp. 1690–1705, Aug. 2003.

[12] X. Li, S. K. Davis, S. C. Hagness, D. W. van der Weide, and B. D. Van Veen, "Microwave imaging via space time beamforming: Experimentalinvestigation of tumour detection in multilayer breast phantoms," IEEE Trans. Microw. Theory Tech., vol. 52, no. 8, pp. 1856–1865, Aug. 2004.

[13] E. C. Fear and J. Sill, "Preliminary investigations of tissue sensing adaptive radar for breast tumour detection," in Proc. Engineering Medicine and Biology Society, Cancun, Mexico, Sep. 2003, pp. 3787–3790.

[14] J. M. Sill and E. C. Fear, "Tissue sensing adaptive radar for breast cancer detection: A study of immersion liquid," Electron. Lett., vol. 41, no. 3, pp. 113–115, Feb. 2005.

[15] J. M. Sill, T. C.Williams, and E. C. Fear, "Tissue sensing adaptive radar for breast tumour detection: Investigation of issues for system implementation," in Int. Zurich Electromagnetic Compatibility Symp., Zurich, Switzerland, Feb. 2005, pp. 71–74.

[16] E. C. Fear, J. Sill, and M. A. Stuchly, "Experimental feasibility study of confocal microwave imaging for breast tumor detection," IEEE Trans. Microw. Theory Tech., vol. 51, no. 3, pp. 887–892, Mar. 2003.

[17] , "Experimental feasibility of breast tumor detection and localization," in IEEE MTT-S Int. Microwave Symp. Dig., Philadelphia, PA, Jun. 2003, pp. 383–386.

[18] J. M. Sill and E. C. Fear, "Tissue sensing adaptive radar for breast cancer detection: Preliminary experimental results," in IEEE MTT-S Int. Microwave Symp. Dig., Long Beach, CA, Jun. 2005. [CD ROM].

[19] E. C. Fear and M. A. Stuchly, "Microwave system for breast tumor detection," IEEE Microw. Guided Wave Lett., vol. 9, no. 11, pp. 470–472, Nov. 1999.

[20] D. M. Hagl, D. Popovic, S. C. Hagness, J. H. Booske, and M. Okoniewski, "Sensing volume of open-ended coaxial probes for dielectric characterization of breast tissue at microwave frequencies," IEEE Trans. Microw. Theory Tech., vol. 51, no. 4, pp. 1194–1206, Apr. 2003.

[21] J. J.W. Lagendijk and P. Nilsson, "Hyperthermia dough: A fat and bone equivalent phantom to test microwave/radio frequency hyperthermia heating systems," Phys. Med. Biol., vol. 30, no. 7, pp. 709–712, 1985.

[22] X. Yun, E. C. Fear, and R. Johnston, "Compact antenna for radar-based breast cancer detection," IEEE Trans. Antennas Propag., vol. 53, no. 8, pp. 2374–2380, Aug. 2005.

[23] K. R. Foster and H. P. Schwan, "Dielectric properties of tissues and biological materials: A critical review," Crit. Rev. Biomed. Eng., vol. 17, no. 1, pp. 25–104, 1989.

[24] T.Wu and R. King, "The cylindrical antenna with nonreflecting resistive loading," IEEE Trans. Antennas Propag., vol. AP-13, no. 3, pp. 369–373, May 1965.

[25] , "Corrections to 'The cylindrical antenna with nonreflecting resistive loading'," IEEE Trans. Antennas Propag., vol. AP-13, no. 11, p. 998, Nov. 1965.

[26] C. D. Woody, "Characterization of an adaptive filter for the analysis of variable latency neuroelectric signals," Med. Biol. Eng., vol. 5, no. 6, pp. 539–553, 1967.

[27] S. Haykin, Adaptive Filter Theory. Upper Saddle River, NJ: Prentice- Hall, 1996.

[28] E. C. Fear, X. Li, S. C. Hagness, and M. A. Stuchly, "Confocal microwave imaging for breast cancer detection: Localization of tumors in three dimensions," IEEE Trans. Biomed. Eng., vol. 49, no. 8, pp. 812–822, Aug. 2002.

[29] J. M. Sill, "Second generation experimental system for tissue sensing adaptive radar," M.S. thesis, Univ. Calgary, Calgary, AB, Canada, 2005.

[30] J. G. Maloney and G. S. Smith, "A study of transient radiation from the Wu–King resistive monopole—FDTD analysis and experimental measurements," IEEE Trans. Antennas Propag., vol. 41, no. 5, pp. 668–676,May 1993.

[31] C. A. Balanis, Antenna Theory: Analysis and Design. New York: Wiley, 1997.

[32] A. Taflove and S. C. Hagness, Computational Electrodynamics: The Finite Difference Time Domain Method. Boston, MA: Artech House, 2000.

[33] D. W. Winters, E. J. Bond, S. C. Hagness, and B. D. Van Veen, "Estimation of average breast tissue properties at microwave frequencies using a time-domain inverse scattering technique," in Int. Zurich Electromagnetic Compatibility Symp., Zurich, Switzerland, Feb. 2005, pp. 59–64.